


Optical classification of excitonic phases in molecular functionalized atomically-thin semiconductorsDominik Christiansen,¹ Malte Selig,¹ Mariana Rossi ,^{2,3} and Andreas Knorr¹¹*Institut für Theoretische Physik, Nichtlineare Optik und Quantenelektronik, Technische Universität Berlin, 10623 Berlin, Germany*²*Max Planck Institute for the Structure and Dynamics of Matter, 22761 Hamburg, Germany*³*Fritz Haber Institute of the Max Planck Society, 14195 Berlin, Germany*

(Received 7 December 2021; revised 5 December 2022; accepted 8 December 2022; published 9 January 2023)

The excitonic insulator is an elusive electronic phase exhibiting a correlated excitonic ground state. Materials with such a phase are expected to have intriguing properties such as excitonic high-temperature superconductivity. However, compelling evidence on the experimental realization is still missing. Here, we theoretically propose hybrids of two-dimensional semiconductors functionalized by organic molecules as prototypes of excitonic insulators, with the exemplary candidate WS₂-F6TCNNQ. This material system exhibits an excitonic insulating phase at room temperature with a ground state formed by a condensate of interlayer excitons. To address an experimentally relevant situation, we calculate the corresponding phase diagram for the important parameters: temperature, gap energy, and dielectric environment. Further, to guide future experimental detection, we show how to optically characterize the different excitonic phases via far-infrared to terahertz spectroscopy valid also for monolayer materials.

DOI: [10.1103/PhysRevB.107.L041401](https://doi.org/10.1103/PhysRevB.107.L041401)

Introduction. The excitonic insulator (EI) is a charge neutral, strongly interacting insulating phase that arises from spontaneous formation of excitons [1,2]. The insulating phase is anticipated to appear in semiconductors at thermodynamic equilibrium, as long as the predicted exciton binding energy exceeds the band gap. It presents an interesting platform for realizing many-body ground states of condensed bosons in solids. Although the concept has been known for almost 60 years, to date compelling experimental evidence of the excitonic insulator is still missing. Since the EI phase is predicted to host many novel properties, such as superfluidity [3,4], excitonic high-temperature superconductivity [5,6], and exciton condensation, breakthroughs in finding this new class of insulators has attracted great attention over the past decades [6–11].

There are a few materials, which are suspected to possess EI ground states in a solid state, among others 1T-TiSe₂, WTe₂, Ta₂NiSe₅, or TmSe_{0.45}Te_{0.55} [11–20]. However, it has been difficult to establish whether the EI state has been realized, because the expected electronic phase transition is accompanied by a structural phase transition, which makes it difficult to distinguish between EI and normal insulator or Peierls transition [21–24]. Just recently, the discussion started about EIs in TMDC heterostructures [16,25–27]. A promising candidate is a combination of WSe₂ monolayer and WSe₂/WS₂-moiré bilayer suggested by Gu *et al.* [28]. However, also for these recent TMDC heterostructures the experimental observables leave room for interpretation concerning the nature of the suspected phase.

In this Letter, we present a blueprint for the realization of an EI based on the interlayer excitons of hybrid inorganic-organic systems (HIOS) and present an unambiguous characterization of the EI phase via linear absorption

spectroscopy. HIOS is a growing field with increasing technological importance because it combines the best of two worlds: the strong light-matter interaction/tunability of the transition energies of organic molecules with the high carrier mobility of inorganic semiconductors [29–32]. For the construction of an EI, the low dielectric constant of the molecular lattices [33] and the strong localization of their electrons are excellent conditions for large exciton binding energies of HIOS interface excitons. By that, the investigated HIOS resembles the suggested monolayer/moiré-bilayer system [28]. In particular, the functionalization of atomically-thin semiconductors with organic molecules allows one to choose a material combination with a band gap in an appropriate range [34,35] and the spatial indirect character of the exciton allows for static dipoles and thus unambiguous fine-tuning via static Stark shifts [36]. At the same time, the energy level tunability of the molecular layer has advantages over TMDC bilayer or heterobilayers, where the EI phase is still under discussion [16,25–27].

Figure 1(a) depicts the investigated HIOS with interlayer dispersion close to the K point. The relevant electronic interlayer transition for the EI built up occurs between TMDC valence and molecular conduction band highlighted by the dashed line box. Due to the direct-gap character of the heterostructure dispersion, we also circumvent the formation of Peierls charge density waves. Depending on the interlayer band gap three different excitonic phases can be expected: semimetal, semiconductor, and EI; cf. Figs. 1(b)–1(d). Most importantly, we will show that all three phases can be distinguished by far-infrared/ terahertz (THz) absorption: the semimetal phase exhibits a vanishing or negative band gap with a free electron gas as ground state; cf. Fig. 1(b). The optical response will then be determined by the Drude model

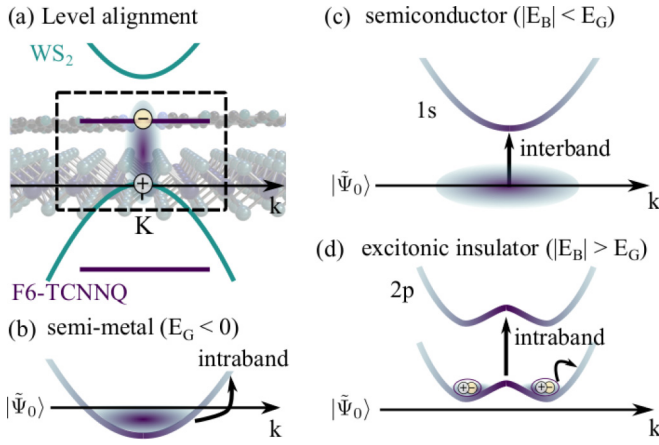


FIG. 1. (a) HIOS consists of monolayers of WS₂ and F6-TCNNQ molecules with level alignment in the free-particle picture. (b)–(d) The interlayer gap dispersion of the dashed boxed for the three possible excitonic phases and the character of their optical excitation.

known from metals [37]. The semiconducting phase, cf. Fig. 1(c), is determined by an exciton binding energy smaller than the free-particle band gap resulting in a filled valence band as ground state. The optical response is given as Lorentz response, however, due to the interlayer character of the transition with considerably small oscillator strength [38,39]. In contrast, the excitonic insulating phase, cf. Fig. 1(d), occurs if the expected exciton binding energy is larger than the band gap. We will exploit that the far-infrared response of such EIs are characterized by transitions in the exciton ladder [40,41] of condensed ground state excitons to higher bound states. With this, we suggest a simple and easy to interpret experiment to characterize the EI built up, which is applicable to monolayers and heterostructures.

In the following, even without applied electric field for energy band fine-tuning, we predict an EI from a hybrid structure of a WS₂ monolayer and a self-assembled layer of F6-TCNNQ molecules. The organic molecules form a periodic two-dimensional lattice, where we investigate the realistic ratio of one molecule per 16 WS₂ unit cells due to the weak molecule-WS₂ interaction [42]. From first-principles calculations we find a type-II band alignment heterostructure with an interlayer gap between the WS₂ valence band and the F6-TCNNQ lowest unoccupied molecular orbital of $E_G = 0.12$ eV [43]. The naively calculated interlayer exciton binding energy, using well documented methods [44], with completely filled valence band as ground state is 0.14 eV. This is on the same order of magnitude as the band gap of 0.12 eV, indicating the possibility of forming a strongly correlated insulating phase to minimize energy.

Ground state of EI. To calculate the EI ground state, we diagonalize the field-independent part of the mean-field Hamiltonian (cf. the Supplemental Material SM [45]) by a Bogoliubov transformation [46,47] with $\alpha_{\mathbf{k}}^{\dagger} = u_{\mathbf{k}}^* v_{\mathbf{k}}^{\dagger} - w_{\mathbf{k}}^* c_{\mathbf{k}}^{\dagger}$ and $\beta_{\mathbf{k}}^{\dagger} = w_{\mathbf{k}} v_{\mathbf{k}}^{\dagger} + u_{\mathbf{k}} c_{\mathbf{k}}^{\dagger}$ [2,48,49]. The fermionic operators $\alpha_{\mathbf{k}}^{\dagger}$ and $\beta_{\mathbf{k}}^{\dagger}$ create an electron in a linear combination of valence $v_{\mathbf{k}}^{(\dagger)}$ and conduction $c_{\mathbf{k}}^{(\dagger)}$ bands in analogy to the Bogoliubov particle operators from BCS superconductivity theory. The

diagonalized Hamiltonian reads $H = \sum_{n=\{\alpha,\beta\},\mathbf{k}} E_{n,\mathbf{k}} n_{\mathbf{k}}^{\dagger} n_{\mathbf{k}}$ with the hybridized bands $E_{\alpha/\beta,\mathbf{k}} = (\tilde{\varepsilon}_{c,\mathbf{k}} + \tilde{\varepsilon}_{v,\mathbf{k}})/2 \mp \sqrt{\Sigma_{\mathbf{k}}^2 + \Delta_{\mathbf{k}}^2}$. The excitation spectrum of the new quasiparticles corresponds to the Bogoliubov dispersion $E_{\mathbf{k}} = \sqrt{\Sigma_{\mathbf{k}}^2 + \Delta_{\mathbf{k}}^2}$, where the gap dispersion is defined as $\Sigma_{\mathbf{k}} = (\tilde{\varepsilon}_{c,\mathbf{k}} - \tilde{\varepsilon}_{v,\mathbf{k}})/2$. The quantity $\Delta_{\mathbf{k}}$ is determined via the transcendental gap equation [50–52]

$$\Delta_{\mathbf{k}} = \frac{1}{2} \sum_{\mathbf{k}'} V_{\mathbf{k}-\mathbf{k}'} \frac{\Delta_{\mathbf{k}'}}{\sqrt{\Sigma_{\mathbf{k}'}^2 + \Delta_{\mathbf{k}'}^2}} (f_{\alpha,\mathbf{k}'} - f_{\beta,\mathbf{k}'}), \quad (1)$$

$$2\Sigma_{\mathbf{k}} = \varepsilon_{c,\mathbf{k}} - \varepsilon_{v,\mathbf{k}} + \sum_{\mathbf{k}'} \mathcal{V}_{\mathbf{k}-\mathbf{k}'}^{\text{mol}} (u_{\mathbf{k}'}^2 f_{\beta,\mathbf{k}'} + w_{\mathbf{k}'}^2 f_{\alpha,\mathbf{k}'}) - \sum_{\mathbf{k}'} \mathcal{V}_{\mathbf{k}-\mathbf{k}'}^{\text{WS}_2} (u_{\mathbf{k}'}^2 f_{\alpha,\mathbf{k}'} + w_{\mathbf{k}'}^2 f_{\beta,\mathbf{k}'}). \quad (2)$$

The quantity $\Delta_{\mathbf{k}}$ can be identified as ordering parameter determining the phase of the heterostructure. A finite value accounts for a finite probability to create electron-hole pairs, which designates the excitonic instability. In the limit $\Delta_{\mathbf{k}} \rightarrow 0$ the dipolar excitonic insulator [28,53,54] converts to the conventional phases of semiconductor or semimetal depending on the band gap. In Eqs. (1) and (2) we defined the matrix element $\mathcal{V}_{\mathbf{k}-\mathbf{k}'}^l = V_0^l - V_{\mathbf{k}-\mathbf{k}'}^l - V_0 + V_{\mathbf{k}-\mathbf{k}'}$ with intralayer Coulomb potential $V_{\mathbf{k}}^l$ ($l = \{\text{molecule}, \text{WS}_2\}$) and interlayer potential $V_{\mathbf{k}}$ [55]. Equations (1) and (2) depend on the occupa-

tions of the hybridized bands $f_{n,\mathbf{k}} = \langle n_{\mathbf{k}}^{\dagger} n_{\mathbf{k}} \rangle$. The temperature $T = 0$ K limit of the gap equation, i.e., $f_{\alpha,\mathbf{k}} - f_{\beta,\mathbf{k}} = 1$, can also be obtained from a minimization of the energy [51,52]. Clearly, the magnitude of the ordering parameter $\Delta_{\mathbf{k}}$ depends on band gap and temperature, which enters via the Fermi functions $f_{\alpha/\beta,\mathbf{k}}$ of the hybridized bands $E_{\alpha/\beta,\mathbf{k}}$. The chemical potential is chosen such that the charge density is a conserved quantity as function of temperature and band gap. In our case, we consider a charge neutral structure, i.e., the density of holes in WS₂ equals the density of electron in the molecule. Because the ordering parameter enters also in the gap dispersion $\Sigma_{\mathbf{k}}$ via the Fermi functions $f_{n,\mathbf{k}}(E_{n,\mathbf{k}})$, both quantities have to be solved simultaneously and form a temperature-dependent extension of the EI gap equation from literature including now electron and hole Coulomb band renormalizations. If not stated otherwise we use an hBN substrate ($\epsilon = 4.5$) entering the Coulomb potential and a surrounding of air ($\epsilon = 1$) for the numerical evaluation.

Figure 2(a) displays the numerical solution of $\Delta_{\mathbf{k}}$ and $\Sigma_{\mathbf{k}}$ at room temperature and the resulting Bogoliubov dispersion $E_{\mathbf{k}}$ with the original band gap of 0.12 eV. The ordering parameter $\Delta_{\mathbf{k}}$ is symmetric to $k = 0$ and displays a monotonous decrease with the wave number, comparable to the gap function of s -wave superconductors [56–58]. Together with $\Sigma_{\mathbf{k}}$ it yields a sombrero-like Bogoliubov dispersion. We stress that Fig. 2(a) displays the results for 300 K already suggesting that the excitonic condensate is stable up to room temperature. Finally, Fig. 2(a) displays also the gap dispersion $\Sigma_{\mathbf{k}}$. For the discussion of the gap dispersion, it is convenient to introduce the spontaneously forming inversion $f_{\mathbf{k}}^{(0)} \equiv$

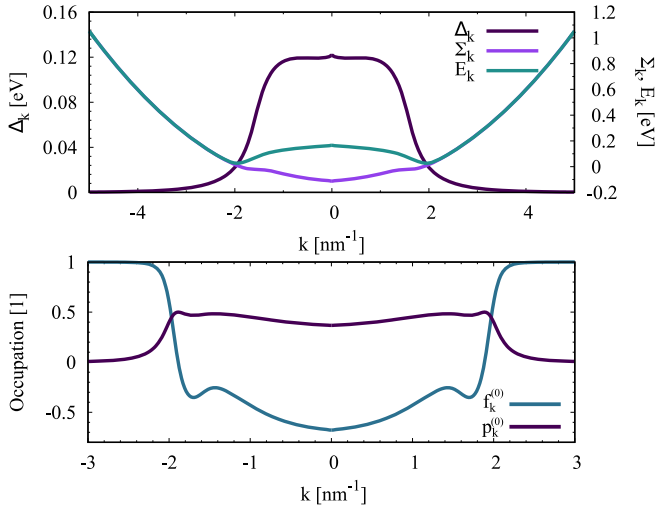


FIG. 2. (a) Numerical solution of the ordering parameter $\Delta_{\mathbf{k}}$ and gap dispersion $\Sigma_{\mathbf{k}}$ as function of wave number at room temperature. Both quantities constitute the Bogoliubov dispersion $E_{\mathbf{k}}$. (b) The EI exhibits a nonvanishing coherence and an intrinsic inversion. The coherence and occupations peak in the pocket of the Bogoliubov dispersion.

$f_{v,\mathbf{k}}^{(0)} - f_{c,\mathbf{k}}^{(0)} = \Sigma_{\mathbf{k}} / \sqrt{\Sigma_{\mathbf{k}}^2 + \Delta_{\mathbf{k}}^2} (f_{\alpha,\mathbf{k}} - f_{\beta,\mathbf{k}})$ and the macroscopic coherence $p_{\mathbf{k}}^{(0)} = \langle v_{\mathbf{k}}^{\dagger} c_{\mathbf{k}} \rangle^{(0)} = \frac{1}{2} \Delta_{\mathbf{k}} / \sqrt{\Sigma_{\mathbf{k}}^2 + \Delta_{\mathbf{k}}^2} (f_{\alpha,\mathbf{k}} - f_{\beta,\mathbf{k}})$ forming without external source and plotted in Fig. 2(b). Here, in contrast to a conventional semiconductor ($\Delta_{\mathbf{k}} = 0$) for $\Delta_{\mathbf{k}} \neq 0$, the ground state coherence $p_{\mathbf{k}}^{(0)}$ has a nonvanishing value and the occupation inversion deviates from unity clarifying why $\Delta_{\mathbf{k}}$ is referred to as ordering parameter. Due to the Hartree-Fock renormalizations the gap dispersion $\Sigma_{\mathbf{k}}$ turns negative; cf. Fig. 2(a). This leads to an intrinsic inversion $f_{\mathbf{k}}^{(0)} < 0$ close to the band extremum. From Fig. 2(b) we see that the ground state coherence and occupations peak within the pockets of the Bogoliubov dispersion, which we can identify with the Fermi wave number k_F .

Phase diagram. Depending on the two external parameters temperature and band gap affecting the ordering parameter we can expect three different excitonic phases: EI, semiconductor, and semimetal; cf. Figs. 1(b)–1(d). While the EI phase is present for a finite ordering parameter $\Delta_{\mathbf{k}}$, the other two phases reveal a vanishing $\Delta_{\mathbf{k}}$. However, semimetal and semiconductor can be distinguished via the inversion $f_{\mathbf{k}}^{(0)}$: while for a conventional semiconductor the inversion is one in the ground state, the value is smaller than one for a semimetal reflecting the presence of a free electron gas. Figure 3(a) shows the calculated phase diagram of a WS₂-F6TCNNQ stack on hBN substrate as a function of temperature and band gap. As guidance we include the coexistence lines between the different phases. We find that the excitonic insulating phase is stable for temperatures up to 350 K underlining the ability of our proposed structure as high-temperature EI. The EI phase appears in the band gap range of 0.04 eV to 0.38 eV. We see that by increasing the band gap the heterostructure enters its semiconducting phase. When decreasing the band gap we approach the semimetal limit. Interestingly, we find no coex-

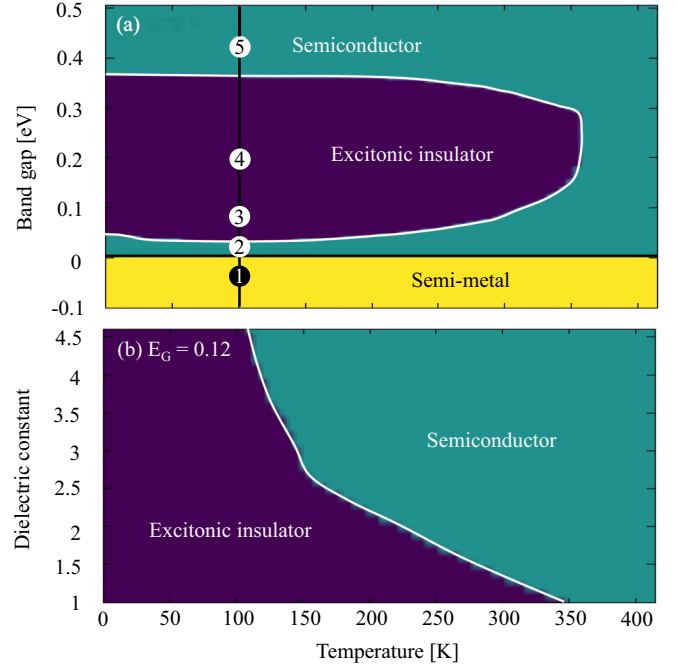


FIG. 3. (a) Phase diagram of a WS₂-F6TCNNQ stack on hBN and air surrounding. The EI phase is separated from the semimetal by the semiconducting phase. The numbers denote the position for the absorption spectra in Fig. 4. Number 3 corresponds to zero applied field. (b) Phase diagram of the WS₂-F6TCNNQ stack on hBN and altering substrate, characterized by the dielectric constant. Environments with low dielectric constant are favorable to stabilize the excitonic insulating phase at higher temperature.

istence line between EI and semimetal, but the heterostructure traverses the semiconducting phase again. This results from a comparably fast decrease of the ordering parameter, vanishing prior to a negative band gap, due to the coupling of Eqs. (1) and (2) via the Coulomb renormalizations. The corresponding separating area between EI and semimetal could be understood as an excited semiconducting phase ($\Delta_{\mathbf{k}} = 0$, $E_{\mathbf{k}} = \tilde{\epsilon}_{c,\mathbf{k}} - \tilde{\epsilon}_{v,\mathbf{k}} > 0$ as in the semiconducting phase but with $f_{c,\mathbf{k}} \neq 0$, $f_{\mathbf{k}}^{(0)} < 1$). Therefore, the transition from the EI in this region of the phase diagram shows similarities with a Mott transition. To change between all three phases a band gap change of 0.12 eV is necessarily possible with an applied voltage of around 5 V [36]. Finally, we see a sublimation line at high enough temperature—a direct transition from semiconductor to semimetal. The billiard balls in Fig. 3(a) are discussed later together with Fig. 4.

We stress that the phase diagram strongly depends on the dielectric environment influencing the interlayer Coulomb potential [55]: in Fig. 3(b) we show the phases for the fixed original band gap of 0.12 eV with altering temperature and dielectric surrounding. The WS₂-F6TCNNQ stack is still placed on top of an hBN substrate, but the dielectric constant of a top layer is changed from vacuum to hBN encapsulation: the stability of the condensate for higher temperature rapidly decreases with increasing dielectric constant. Obviously, a dielectric environment with low mean dielectric constant is favorable to stabilize the EI phase at high temperatures.

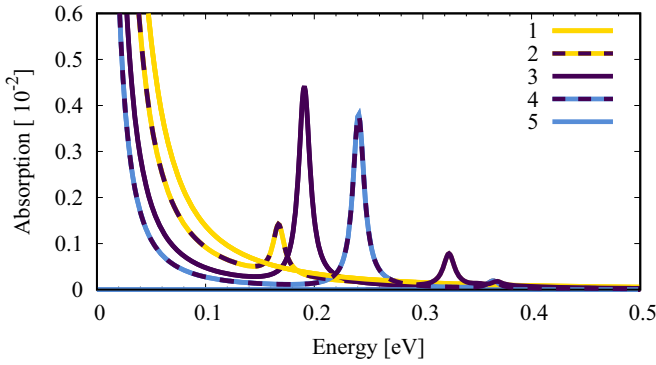


FIG. 4. Absorption spectrum at 100 K along the dotted line in Fig. 3(a). The Drude response in the semimetal phase is modulated by a p -exciton Rydberg series for the EI phase. In the semiconducting phase the terahertz response vanishes.

Optical response. Based on the ground state calculations, we can now calculate the frequency-dependent absorption coefficient via a self-consistent coupling of material and wave equation [59–61]. The linear absorption with respect to the dynamical field $\mathbf{E}(t)$ is determined by the susceptibility described by the microscopic polarization $p_{\mathbf{k}}$ and occupations $f_{\mathbf{k}}$. Both quantities are expanded up to first order in the exciting electric field [52,62,63]. The initial conditions arise from the ground state (initially calculated $p_{\mathbf{k}}^{(0)}$ and $f_{\mathbf{k}}^{(0)}$). The dynamical correction to first order in $\mathbf{E}(t)$ is denoted by $p_{\mathbf{k}}^{(1)}$ and $f_{\mathbf{k}}^{(1)}$. The Heisenberg equation of motion for the microscopic polarization $p_{\mathbf{k}}^{(1)}$ can be diagonalized exploiting the Bogoliubov-Wannier equation [25,62,64]. After diagonalization, based on a $1s$ ground state, it describes transitions to higher lying excitonic states μ with their excitonic energy E_{μ} and wave function $\varphi_{\mu,\mathbf{k}}$. Consequently, the microscopic polarization can be expressed as excitonic polarization $p_{\mu} = \sum_{\mathbf{k}} \varphi_{\mu,\mathbf{k}}^* p_{\mathbf{k}}^{(1)}$ [40,65,66] (details in the SM [67]). A direct solution of the Heisenberg equations of motion for excitonic polarization and excited occupation in frequency domain yields the susceptibility, detectable in far-infrared/THz experiments:

$$\chi(\omega) = -\frac{1}{\epsilon_0} \sum_{\mu} \frac{\mathbf{d}_{\mu} \otimes \mathbf{d}_{\mu} + \mathbf{j}_{\mu} \otimes \mathbf{j}_{\mu}}{\hbar\omega - E_{\mu} + i\gamma} + \frac{e_0^2}{\epsilon_0 \hbar} \sum_{\mathbf{k}} \frac{\mathbf{v}_{\mathbf{k}} \otimes \nabla_{\mathbf{k}} f_{v,\mathbf{k}}^{(0)}}{\omega^2 + i\gamma\omega/\hbar}, \quad (3)$$

with the particle velocity $\mathbf{v}_{\mathbf{k}} = \hbar\mathbf{k}/m$, elementary charge e_0 , and valence electron mass m . The excitonic *interband* matrix element reads $\mathbf{d}_{\mu} = \mathbf{d} \sum_{\mathbf{k}} f_{\mathbf{k}}^{(0)} \varphi_{\mu,\mathbf{k}}^*$ with electronic dipole moment \mathbf{d} . The second summand is driven by the excitonic *intra*band matrix element $\mathbf{j}_{\mu} = e_0 \cdot \sum_{\mathbf{k}} \varphi_{\mu,\mathbf{k}}^* \nabla_{\mathbf{k}} p_{\mathbf{k}}^{(0)}$. Both contributions exhibit resonances at the exciton energy E_{μ} . For an EI with s -symmetric ground state the first excited exciton is of p symmetry, that we can expect the $1s$ - $2p$ transition as the energetically lowest resonance [40,41]. For a p -excited state [$\mu = p$ in Eq. (3)], the interband source vanishes because of its uneven parity. In contrast, the intra

band source is finite. When entering the semiconducting phase, the Bogoliubov-Wannier equation yields as lowest excited state $1s$ excitons. In this phase, the optical source is of interband nature from a fully occupied valence band as ground state; cf. Fig. 1(c). In contrast the intra

band source vanishes due to symmetry reasons. Additionally, $f_{v,\mathbf{k}}^{(0)} = 1$ (full valence band) now holds that the third term in Eq. (3), which resembles the conductivity tensor of a plasma, vanishes. Finally, for zero or negative band gap the heterostructure is in its semimetallic phase and the optical matrix elements \mathbf{d}_{μ} and \mathbf{j}_{μ} are zero due to the corresponding ground state coherence and inversion. The optical response is now solely described by the third term in Eq. (3). We can perform a partial integration to bring the third term in the susceptibility into the form $\chi_{\text{Drude}}(\omega) = \omega_{pl}^2 / (\omega^2 + i\gamma\omega/\hbar)$, which corresponds to the plasma response in a Drude model for a free electron gas; cf. Fig. 1(b). It stems from intra

exciton extension a_X [71]. Although this value lies below the Mott transition [72,73], the density is comparably high [74] not ruling out an EHL formation [73,75]. However, the appearance of an EHL or EI can be distinguished in the optical experiment. While the EI shows a linear response due to a substantial oscillator from intraband transitions, the spectral signature of the EHL should be vanishing small due to interband transitions. In any case the EHL response should also be strongly blueshifted to the EI signal due to Pauli blocking and Coulomb shifts. A critical discussion on EHLs is found in the SM [76].

Conclusion. In summary, we propose HIOS as a candidate for the realization of an EI exploiting interlayer excitons. Additional static fields can be used for fine-tuning or to induce different excitonic phases. We show that Coulomb renormalizations have a drastic influence on the excitonic ordering and should always be considered. The occurring optical far-infrared/THz response can be used to character-

ize the excitonic phases: while the conventional interlayer semiconductor exhibits an s -like Rydberg series with minimal oscillator strength, the EI's Rydberg series has p character with strong oscillator strength including a Drude-like response from the ground state occupation. Concluding, the optical response provides a clear signature of the nature of the respective excitonic phase. Finally, we want to stress that an extension beyond the Hartree-Fock limit allows a more precise estimation of the critical temperature. However, this has no influence on the optical response.

Acknowledgments We thank K. Bolotin (FU Berlin), F. von Oppen (FU Berlin), and S. Reich (FU Berlin) for fruitful discussions. Additionally, we appreciate the discussions with F. Katsch, M. Katzer, and L. Greten (TU Berlin). We acknowledge financial support from the Deutsche Forschungsgemeinschaft (DFG) through SFB 951 (D.C., M.S., M.R., and A.K.) Project No. 182087777. D.C. thanks the graduate school Advanced Materials (SFB 951) for support.

-
- [1] L. Keldysh and Y. V. Kopayev, *Sov. Phys. Solid State, USSR* **6**, 2219 (1965).
- [2] D. Jérôme, T. Rice, and W. Kohn, *Phys. Rev.* **158**, 462 (1967).
- [3] S. Gupta, A. Kutana, and B. I. Yakobson, *Nat. Commun.* **11**, 2989 (2020).
- [4] E. Perfetto and G. Stefanucci, *Phys. Rev. B* **103**, L241404 (2021).
- [5] R. Parmenter and W. Henson, *Phys. Rev. B* **2**, 140 (1970).
- [6] R. Wang, O. Erten, B. Wang, and D. Xing, *Nat. Commun.* **10**, 210 (2019).
- [7] D. Varsano, S. Sorella, D. Sangalli, M. Barborini, S. Corni, E. Molinari, and M. Rontani, *Nat. Commun.* **8**, 1461 (2017).
- [8] E. Perfetto, D. Sangalli, A. Marini, and G. Stefanucci, *Phys. Rev. Mater.* **3**, 124601 (2019).
- [9] E. Perfetto, A. Marini, and G. Stefanucci, *Phys. Rev. B* **102**, 085203 (2020).
- [10] E. Perfetto and G. Stefanucci, *Phys. Rev. Lett.* **125**, 106401 (2020).
- [11] Y. Jia, P. Wang, C.-L. Chiu, Z. Song, G. Yu, B. Jäck, S. Lei, S. Klemenz, F. A. Cevallos, M. Onyszczak *et al.*, *Nat. Phys.* **18**, 87 (2022).
- [12] D. Varsano, M. Palumbo, E. Molinari, and M. Rontani, *Nat. Nanotechnol.* **15**, 367 (2020).
- [13] H. Cercellier, C. Monney, F. Clerc, C. Battaglia, L. Despont, M. G. Garnier, H. Beck, P. Aebi, L. Patthey, H. Berger, and L. Forro, *Phys. Rev. Lett.* **99**, 146403 (2007).
- [14] C. Monney, E. Schvier, M. G. Garnier, N. Mariotti, C. Didiot, H. Cercellier, J. Marcus, H. Berger, A. Titov, H. Beck *et al.*, *New J. Phys.* **12**, 125019 (2010).
- [15] Y. Wakisaka, T. Sudayama, K. Takubo, T. Mizokawa, M. Arita, H. Namatame, M. Taniguchi, N. Katayama, M. Nohara, and H. Takagi, *Phys. Rev. Lett.* **103**, 026402 (2009).
- [16] Y. F. Lu, H. Kono, T. I. Larkin, A. W. Rost, T. Takayama, A. V. Boris, B. Keimer, and H. Takagi, *Nat. Commun.* **8**, 14408 (2017).
- [17] D. Werdehausen, T. Takayama, M. Höppner, G. Albrecht, A. W. Rost, Y. Lu, D. Manske, H. Takagi, and S. Kaiser, *Sci. Adv.* **4**, eaap8652 (2018).
- [18] B. Bucher, P. Steiner, and P. Wächter, *Phys. Rev. Lett.* **67**, 2717 (1991).
- [19] F. X. Bronold and H. Fehske, *Phys. Rev. B* **74**, 165107 (2006).
- [20] K. Fukutani, R. Stania, C. I. Kwon, J. S. Kim, K. J. Kong, J. Kim, and H. W. Yeom, *Nat. Phys.* **17**, 1024 (2021).
- [21] K. Rossnagel, L. Kipp, and M. Skibowski, *Phys. Rev. B* **65**, 235101 (2002).
- [22] B. Zenker, H. Fehske, and H. Beck, *Phys. Rev. B* **90**, 195118 (2014).
- [23] Z. Jiang, Y. Li, S. Zhang, and W. Duan, *Phys. Rev. B* **98**, 081408(R) (2018).
- [24] P. A. Volkov, M. Ye, H. Lohani, I. Feldman, A. Kanigel, and G. Blumberg, *Phys. Rev. B* **104**, L241103 (2021).
- [25] S. S. Ataei, D. Varsano, E. Molinari, and M. Rontani, *Proc. Natl. Acad. Sci. USA* **118**, e20110118(2021).
- [26] L. Ma, P. X. Nguyen, Z. Wang, Y. Zeng, K. Watanabe, T. Taniguchi, A. H. MacDonald, K. F. Mak, and J. Shan, *Nature (London)* **598**, 585 (2021).
- [27] Z. Zhang, E. C. Regan, D. Wang, W. Zhao, S. Wang, M. Sayyad, K. Yumigeta, K. Watanabe, T. Taniguchi, S. Tongay *et al.*, *Nat. Phys.* **18**, 1214 (2022).
- [28] J. Gu, L. Ma, S. Liu, K. Watanabe, T. Taniguchi, J. C. Hone, J. Shan, and K. F. Mak, *Nat. Phys.* **18**, 395 (2022).
- [29] J. Sun, Y. Choi, Y. J. Choi, S. Kim, J.-H. Park, S. Lee, and J. H. Cho, *Adv. Mater.* **31**, 1803831 (2019).
- [30] Z. Song, T. Schultz, Z. Ding, B. Lei, C. Han, P. Amsalem, T. Lin, D. Chi, S. L. Wong, Y. J. Zheng *et al.*, *ACS Nano* **11**, 9128 (2017).
- [31] N. Koch, *ChemPhysChem* **8**, 1438 (2007).
- [32] M. Fahlman, S. Fabiano, V. Gueskine, D. Simon, M. Berggren, and X. Crispin, *Nat. Rev. Mater.* **4**, 627 (2019).
- [33] S. Torabi, F. Jahani, I. Van Severen, C. Kanimozhi, S. Patil, R. W. Havenith, R. C. Chiechi, L. Lutsen, D. J. Vanderzande, T. J. Cleij *et al.*, *Adv. Funct. Mater.* **25**, 150 (2015).
- [34] C. R. Groom, I. J. Bruno, M. P. Lightfoot, and S. C. Ward, *Acta Crystallogr., B: Struct. Sci., Cryst. Eng. Mater.* **72**, 171 (2016).
- [35] A. Stuke, C. Kunkel, D. Golze, M. Todorović, J. T. Margraf, K. Reuter, P. Rinke, and H. Oberhofer, *Sci. Data* **7**, 58 (2020).
- [36] E. Lorchat, M. Selig, F. Katsch, K. Yumigeta, S. Tongay, A. Knorr, C. Schneider, and S. Höfling, *Phys. Rev. Lett.* **126**, 037401 (2021).
- [37] P. Drude, *Ann. Phys. (NY)* **306**, 566 (1900).

- [38] R. Gillen, *Phys. Status Solidi B* **258**, 2000614 (2021).
- [39] T. Deilmann and K. S. Thygesen, *Nano Lett.* **18**, 2984 (2018).
- [40] M. Kira and S. Koch, *Prog. Quantum Electron.* **30**, 155 (2006).
- [41] J. Bhattacharyya, S. Zybell, F. Esser, M. Helm, H. Schneider, L. Schneebeli, C. N. Bottge, B. Breddermann, M. Kira, S. W. Koch, A. M. Andrews, and G. Strasser, *Phys. Rev. B* **89**, 125313 (2014).
- [42] S. Park, H. Wang, T. Schultz, D. Shin, R. Ovsyannikov, M. Zacharias, D. Maksimov, M. Meissner, Y. Hasegawa, T. Yamaguchi *et al.*, *Adv. Mater.* **33**, 2008677 (2021).
- [43] The Kohn-Sham energy levels of F6-TCNNQ and WS₂ were obtained with the range-separated HSE06 hybrid functional [77], as implemented in the FHI-aims program [78–80] and using standard intermediate settings [42,81].
- [44] E. Malic, M. Selig, M. Feierabend, S. Brem, D. Christiansen, F. Wendler, A. Knorr, and G. Berghäuser, *Phys. Rev. Mater.* **2**, 014002 (2018).
- [45] See Supplemental Material at <http://link.aps.org/supplemental/10.1103/PhysRevB.107.L041401> for more details on the Hamiltonian and the diagonalization, which includes Refs. [2,36,55,82].
- [46] N. Bogoljubov, V. V. Tolmachev, and D. Širkov, *Fortschr. Phys.* **6**, 605 (1958).
- [47] J. Valatin, *Nuovo Cimento* **7**, 843 (1958).
- [48] L. Keldysh and A. Kozlov, *Zh. Eksp. Teor. Fiz.* **54**, 978 (1968) [*Sov. Phys. JETP* **27**, 521 (1968)].
- [49] C. Comte and P. Nozieres, *J. Phys. (France)* **43**, 1069 (1982).
- [50] A. Kozlov and L. Maksimov, *J. Exptl. Theoret. Phys. (U.S.S.R.)* **48**, 1184 (1965) [*Sov. Phys. JETP* **21**, 790 (1965)].
- [51] J. Sabio, F. Sols, and F. Guinea, *Phys. Rev. B* **82**, 121413(R) (2010).
- [52] T. Stroucken, J. H. Grönqvist, and S. W. Koch, *Phys. Rev. B* **84**, 205445 (2011).
- [53] R. Zimmermann and C. Schindler, *Solid State Commun.* **144**, 395 (2007).
- [54] C. Schindler and R. Zimmermann, *Phys. Rev. B* **78**, 045313 (2008).
- [55] S. Ovesen, S. Brem, C. Linderålv, M. Kuisma, T. Korn, P. Erhart, M. Selig, and E. Malic, *Commun. Phys.* **2**, 23 (2019).
- [56] J. Bardeen, L. N. Cooper, and J. R. Schrieffer, *Phys. Rev.* **108**, 1175 (1957).
- [57] M. Tinkham, *Introduction to Superconductivity* (Courier Corporation, New York, 2004).
- [58] D. Reyes, M. A. Continentino, C. Thomas, and C. Lacroix, *Ann. Phys. (NY)* **373**, 257 (2016).
- [59] A. Knorr, S. Hughes, T. Stroucken, and S. Koch, *Chem. Phys.* **210**, 27 (1996).
- [60] E. Malic and A. Knorr, *Graphene and Carbon Nanotubes: Ultrafast Optics and Relaxation Dynamics* (John Wiley & Sons, New York, 2013).
- [61] F. Katsch and A. Knorr, *Phys. Rev. X* **10**, 041039 (2020).
- [62] T. Stroucken and S. W. Koch, *J. Phys.: Condens. Matter* **27**, 345003 (2015).
- [63] D. C. Desai, B. Zviazhynski, J.-J. Zhou, and M. Bernardi, *Phys. Rev. B* **103**, L161103 (2021).
- [64] T. Stroucken and S. W. Koch, *Optical Properties of Graphene* (World Scientific, Singapore, 2017), pp. 43–84.
- [65] F. Katsch, D. Christiansen, R. Schmidt, S. M. de Vasconcellos, R. Bratschitsch, A. Knorr, and M. Selig, *Phys. Rev. B* **102**, 115420 (2020).
- [66] S. Dong, M. Puppini, T. Pincelli, S. Beaulieu, D. Christiansen, H. Hübener, C. W. Nicholson, R. P. Xian, M. Dendzik, Y. Deng *et al.*, *Nat. Sci.* **1**, e10010 (2021).
- [67] See Supplemental Material at <http://link.aps.org/supplemental/10.1103/PhysRevB.107.L041401> for more details on the equations of motion and optical response, which includes Refs. [62,83].
- [68] M. Selig, G. Berghäuser, A. Raja, P. Nagler, C. Schüller, T. F. Heinz, T. Korn, A. Chernikov, E. Malic, and A. Knorr, *Nat. Commun.* **7**, 13279 (2016).
- [69] D. Christiansen, M. Selig, G. Berghäuser, R. Schmidt, I. Niehues, R. Schneider, A. Arora, S. M. de Vasconcellos, R. Bratschitsch, E. Malic *et al.*, *Phys. Rev. Lett.* **119**, 187402 (2017).
- [70] S. Helmrich, K. Sampson, D. Huang, M. Selig, K. Hao, K. Tran, A. Achstein, C. Young, A. Knorr, E. Malic *et al.*, *Phys. Rev. Lett.* **127**, 157403 (2021).
- [71] J. Zipfel, J. Holler, A. A. Mitoglu, M. V. Ballottin, P. Nagler, A. V. Stier, T. Taniguchi, K. Watanabe, S. A. Crooker, P. C. M. Christianen, T. Korn, and A. Chernikov, *Phys. Rev. B* **98**, 075438 (2018).
- [72] A. Barman Ray, K. Liang, and A. N. Vamivakas, *Phys. Rev. B* **106**, 045206 (2022).
- [73] P. Pekh, P. Ratnikov, and A. Silin, *JETP* **133**, 494 (2021).
- [74] L. Sigl, M. Troue, M. Katzer, M. Selig, F. Sigger, J. Kiemle, M. Brotons-Gisbert, K. Watanabe, T. Taniguchi, B. D. Gerardot *et al.*, *Phys. Rev. B* **105**, 035417 (2022).
- [75] A. Rustagi and A. F. Kemper, *Nano Lett.* **18**, 455 (2018).
- [76] See Supplemental Material at <http://link.aps.org/supplemental/10.1103/PhysRevB.107.L041401> for a discussion on interlayer excitons and EHLs, which includes Refs. [71–75,84–86].
- [77] A. V. Krukau, O. A. Vydrov, A. F. Izmaylov, and G. E. Scuseria, *J. Chem. Phys.* **125**, 224106 (2006).
- [78] V. Blum, R. Gehrke, F. Hanke, P. Havu, V. Havu, X. Ren, K. Reuter, and M. Scheffler, *Comput. Phys. Commun.* **180**, 2175 (2009).
- [79] X. Ren, P. Rinke, V. Blum, J. Wieferink, A. Tkatchenko, A. Sanfilippo, K. Reuter, and M. Scheffler, *New J. Phys.* **14**, 053020 (2012).
- [80] S. V. Levchenko, X. Ren, J. Wieferink, R. Johanni, P. Rinke, V. Blum, and M. Scheffler, *Comput. Phys. Commun.* **192**, 60 (2015).
- [81] H. Wang, S. V. Levchenko, T. Schultz, N. Koch, M. Scheffler, and M. Rossi, *Adv. Electron. Mater.* **5**, 1800891 (2019).
- [82] S. Dong, S. Beaulieu, M. Selig, P. Rosenzweig, D. Christiansen, T. Pincelli, M. Dendzik, J. D. Ziegler, J. Maklar, R. P. Xian *et al.*, [arXiv:2108.06803](https://arxiv.org/abs/2108.06803).
- [83] M. Selig, F. Katsch, R. Schmidt, S. Michaelis de Vasconcellos, R. Bratschitsch, E. Malic, and A. Knorr, *Phys. Rev. Res.* **1**, 022007(R) (2019).
- [84] Y. Yu, A. W. Bataller, R. Younts, Y. Yu, G. Li, A. A. Puretzy, D. B. Geohegan, K. Gundogdu, and L. Cao, *ACS Nano* **13**, 10351 (2019).
- [85] M. Combescot and P. Nozieres, *J. Phys. C* **5**, 2369 (1972).
- [86] E. Andryushyn and A. Silin, *Solid State Commun.* **20**, 453 (1976).